Author(s): Shi, Hongbo; Koskinen, Pekka; Ramasubramaniam, Ashwin

Title: A Self-Consistent Charge Density-Functional Tight-Binding Parameterization for Pt-Ru Alloys

Year: 2017

Version:

Article

A Self-Consistent Charge Density-Functional Tight-Binding Parameterization for Pt-Ru Alloys

Hongbo Shi, Pekka Koskinen, and Ashwin Ramasubramaniam

Just Accepted

A Self-Consistent Charge Density-Functional Tight-Binding Parameterization for Pt-Ru Alloys

Hongbo Shi,[1] Pekka Koskinen,[2] and Ashwin Ramasubramaniam [3], *

[1] Department of Chemical Engineering,

University of Massachusetts, Amherst, MA 01003, USA

[2] Department of Physics

University of Jyväskylä, 40014, Jyväskylä, Finland

[3] Department of Mechanical and Industrial Engineering,

University of Massachusetts, Amherst, MA 01003, USA

Abstract

We present a self-consistent charge density-functional tight-binding (SCC-DFTB) parameterization for PtRu alloys, which is developed by employing a training set of alloy cluster energies and forces obtained from Kohn-Sham density functional theory (DFT) calculations. Extensive simulations of a testing set of PtRu alloy nanoclusters show that this SCC-DFTB scheme is capable of capturing cluster formation energies with high accuracy relative to DFT calculations. The new SCC-DFTB parameterization is employed within a Genetic Algorithm to search for global minima of PtRu clusters in the range of 13-81 atoms and the emergence of Ru-core/Pt-shell structures at intermediate alloy compositions, consistent with known results, is systematically demonstrated. Our new SCC-DFTB parameterization enables computationally inexpensive and accurate modeling of Pt-Ru clusters that are among the best-performing catalysts in numerous energy applications.

* **Corresponding Author:** ashwin@engin.umass.edu

1

1. INTRODUCTION

Platinum and platinum-group metals serve as important electrocatalysts in hydrogen-based or methanol-based proton-exchange-membrane fuel cells (PEMFC).[1, 2, 3] In spite of the widespread use of these metals, there are still important challenges that need to be met in ensuring catalyst selectivity and durability. For example, carbon monoxide, which is a common impurity in hydrogen feeds or produced as a reaction intermediate, easily poisons the active sites of Pt catalysts.[4, 5, 6, 7] It is well known that by partially alloying Pt with another metal, both CO tolerance and electrocatalytic activity can be improved. For example, PtRu,[4, 8] PtCo,[9, 10] and PtMo[11, 12] alloys have been investigated as anode materials for fuel cells and, currently, PtRu alloy clusters are known to show the highest resistance to CO poisoning and highest catalytic activity in PEMFCs.[2] The superior performance of PtRu over Pt clusters has been explained by invoking the ligand effect,[13, 14] which reduces the binding strength of CO at active sites, as well as a bifunctional mechanism,[15] which accesses alternate pathways of reduced energy barriers for the oxidation and elimination of CO. Yet, there remain important gaps in our systematic understanding of the influence of size, structure, and composition of PtRu alloys on catalytic performance at the nanoscale (alloy nanoclusters).

Computer modeling is a very powerful approach for the study of structure–function relationships in catalysis. In particular, modeling plays a key role in the study of catalyst nanoclusters where direct experimental measurements of structural properties are extremely challenging and sometimes infeasible. An important objective in modeling nanoclusters is to ascertain, for a given size and composition, the morphology that corresponds to the thermodynamic ground state. Thus, significant effort has been devoted to developing robust numerical methods for predicting low-energy structures for various metal clusters.[2, 16, 17, 18, 19, 20] Density functional theory (DFT) is a particularly useful tool for calculating potential energy

2

surfaces and has been widely used for global optimization of nanoscale alloy structures.[19, 21] On

the one hand, DFT requires very few adjustable parameters making it a reliable modeling tool for

most chemical elements. On the other hand, the unfavorable scaling of the method with system

size implies that optimization studies at the DFT level are typically limited to small clusters (10-

100 atoms). Empirical interatomic potentials, which are much less computationally demanding,

can help push the size limit on cluster optimization studies; however, such potentials often suffer

from drawbacks in terms of transferability and possible over-parameterization. In the present

context, we are unaware of widely used, well-tested interatomic potentials for Pt-Ru alloy

clusters, which stymies progress in modeling this important class of catalysts.

Density-functional tight-binding (DFTB) represents another powerful modeling approach

that has been widely employed for studying carbon-based systems[22, 23] and metals with

delocalized valance electrons.[24, 25, 26] Recently, the accuracy of DFTB has been further improved

[27, 28] by adding self-consistent charge (SCC) corrections to take into account charge transfer due

to interatomic interactions. The computational speed of SCC-DFTB is intermediate between

DFT and empirical potential methods thus opening up possibilities for global optimization for

larger clusters sizes with high accuracy. Thus, the primary goal of this paper is to obtain an

accurate set of SCC-DFTB parameters for modeling PtRu alloy clusters. (We use the terms SCC-

DFTB and DFTB interchangeably from here on for convenience.) In the process, of developing a

suitable parameterization for Pt-Ru interatomic interactions, we also obtain an accurate set of

parameters for the homo-elemental Pt-Pt and Ru-Ru interactions, which also do not exist in the

literature to date. Thus, our work contributes an important set of tools for SCC-DFTB modeling

of Pt, Ru, and PtRu clusters that can be employed in a wide range of applications, including

molecular dynamics and structural optimization, while pushing the size limits currently imposed

by more expensive DFT-based approaches.

The remainder of this paper is organized as follows. In Section 2, we provide detailed information of the modeling procedures. In Section 3, we provide the details of the SCC-DFTB fitting procedure careful benchmarking against a DFT testing set. As a sample application, in Section 4, the SCC-DFTB approach is employed within a Genetic Algorithm to search for optimal (low-energy) structures of PtRu clusters at various sizes and compositions. A summary and concluding remarks are provided in Section 5.

2. COMPUTATIONAL METHODS

2.1 SCC-DFTB method

Formally, the total energy, E, of a tight-binding system can be expressed within the DFTB approximation as [24]

$$E = E_{bs} + E_{Coul} + E_{rep}, \tag{1}$$

where E_{bs} is the band structure energy, E_{Coul} is the Coulomb interaction energy and E_{rep} is the repulsive energy. In the DFTB formalism, E_{bs} is obtained simply from the summation of orbital interaction energies, which are typically calculated once and for all for a given set of elements, while E_{Coul} is determined by a single parameter, namely, the Hubbard U parameter. All cumbersome terms related to electron exchange and correlation as well as terms related to ion-ion repulsion are clumped together in the pairwise potential, $V_{rep,I,J}(R_{IJ})$, from which the repulsive energy is obtained as

$$E_{rep} = \sum_{I<J} V_{rep,I,J}(R_{IJ}). \tag{2}$$

The potential function, $V_{rep,I,J}(R_{IJ})$, is treated as an empirical function that is to be determined by fitting to experimental data and/or data from higher-level electronic structure calculations. In

4

this work, we employ training sets obtained from DFT calculations. The details of the fitting

procedure and results of subsequent tests are reported in Section 3. For now, we simply note that

the potential fitting in this work was performed using the Hotbit package.[24, 29] Slater-Koster

parameter tables from Hotbit were converted to the standard DFTB format and the DFTB+

package[30] was used for the testing phase as well as for subsequent global optimization studies. In

the DFTB+ calculations, the electronic temperature was set to 100 K to accelerate electronic

convergence.

2.2 Density functional theory calculations

DFT calculations of PtRu clusters were performed using the Vienna *Ab Initio* Simulation

Package (VASP).[31, 32] Electron exchange and correlation were described using the Perdew-

Burke-Ernzerhof (PBE)[33, 34, 35] form of the generalized-gradient approximation with spin

polarization. A kinetic energy cutoff of 400 eV was used for the plane-wave basis set and a

second-order Methfessel-Paxton[36] smearing with width of 0.05 eV was employed. Brillouin zone

sampling was performed using a single Γ point. Periodic images of clusters were separated by

more than 10 Å of vacuum in all directions to eliminate spurious interactions between periodic

images.

2.3 Genetic Algorithm for structural optimization of alloy clusters

Structural optimization of nanoparticles/clusters can be treated by various approaches such as

basin-hopping,[37, 38, 39, 40, 41] particle-swarm optimization,[42, 43] and genetic algorithms.[16, 44, 45] In

this work, we employ a genetic algorithm (GA) for structural optimization of PtRu clusters.

Since this method has been described exhaustively in our recent work on Pt clusters,[18] we refer

the reader to that work for details; here, we only provide pertinent comments on the crossover and mutation processes that need to be handled differently for alloy clusters as opposed to homo-elemental ones.

Crossover: The two parent clusters were shifted to the origin and rotated, and then sectioned at the $z = 0$ plane. Thereafter, the upper halves from each parent cluster are exchanged and "glued" together to form two child clusters. To ensure that the number of atoms is conserved in this process, the cutting plane might need to be shifted slightly from $z = 0$, depending on the structure of the parent clusters. However, it is difficult to conserve both composition and mass using the same cutting plane. Thus, as a final step in forming the child clusters, we allow for a random exchange of atomic species to restore the overall composition.

Mutation: To avoid stagnation of the GA, all clusters in a new generation are mutated with 20% probability by swapping the atom types of a randomly chosen Pt-Ru pair without additionally perturbing the structure of the cluster. Mutated clusters are then relaxed with local optimization and replace the old clusters.

Convergence is achieved if the total energy of the lowest energy cluster in a new generation differs by less than 0.01 eV/atom from that of the previous generation. In general, evolution to a new generation becomes much slower at the late stages of optimization; thus, it is possible that convergence might not be achievable for larger clusters. In such cases, optimization is stopped if the total number of mating events exceeds 10,000 and the lowest energy structure will be taken as the putative global minimum. While it is impossible to guarantee that the lowest-energy structure found is indeed the global minimum, the GA nevertheless outperforms simulated-annealing tests as reported in Table S2.

6

2.4 Calculation procedures

First, we performed DFT calculations on randomly generated PtRu clusters of varying size (13-81 atoms) and composition to create a large database (approximately 200 samples) of equilibrium (structurally optimized) and non-equilibrium (artificially deformed) structures, energies, and forces. Thereafter, 50% of this database was used as a training set to parameterize DFTB potentials for Pt-Pt, Pt-Ru and Ru-Ru interactions; the remaining 50% of the database was used as a testing set to ascertain the accuracy of the DFTB-predicted energetics relative to DFT. Since the clusters used in the fitting procedure were randomly generated, the ability of the DFTB potentials to predict minimum energy configurations of clusters with accuracy remained to be verified. Therefore, as the second phase of the simulations, the potential energy surface generated by the Pt-Ru DFTB model was sampled using a Genetic Algorithm and minimum energy configurations calculated for a selected set of clusters of varying sizes and compositions (see Table S2). The DFTB-optimized minimum energy clusters were imported into VASP and further minimized using a conjugate-gradient algorithm (local minimization) at the DFT level. The DFTB and DFT results were then compared in terms of cluster formation energies to validate trends across cluster sizes and compositions.

3. RESULTS AND DISCUSSION

3.1 Parameterization and testing of SCC-DFTB potentials

In the first step of potential parameterization, the onsite energies of valence orbitals (ϕ_μ) in free atoms were obtained for calculating the diagonal elements ($H^0_{\mu\mu} = \langle \phi_\mu | H | \phi_\mu \rangle = \varepsilon_{\text{free}}$) of the Hamiltonian matrix. Using the Hotbit package, $\varepsilon_{\text{free}}$ was obtained from all-electron, scalar-relativistic DFT calculations with the PW92 local density approximation[46] for electron exchange and correlation. The onsite energies of the valence orbitals for Pt and Ru are listed in Table 1.

7

The charge transfer energetics can be described within DFTB by a single key parameter, the Hubbard U, with a default value [47] of

$$U \approx IE - EA, \tag{3}$$

where IE is the ionization energy and EA the electronic affinity. The ionization energy and electron affinity are calculated by removing and adding electrons from and to corresponding orbitals of the unconfined atom and then calculating the energy change. Although Hubbard U values can differ by orbital, for simplicity, we use the same U for all orbitals. As the addition of a full electron may destabilize the atom in some cases, only a fraction of an electron is added or removed in practice (0.15 and 0.2 electrons for Pt and Ru d-orbitals, respectively); this is also more representative of the actual degree of charge-transfer in these systems. U values calculated from DFT are listed in Table 1. The charge profiles for atoms were assumed to follow a Gaussian profile.[24]

As free-atom orbital wavefunctions are too diffuse to be considered as basis functions for wavefunction expansion in DFTB, a common strategy to generate more compact orbital basis sets is to model a pseudo-atom, in which an additional confinement is used to mimic the atomic enviroment.[24] We use here a common choice for confinement, namely a quadratic form potential[23]

$$V_{conf}(r) = \left(\frac{r}{r_0}\right)^2, \tag{4}$$

where, as a rule of thumb, r_0 is chosen to be twice the covalent radius. Thus, in the second step of DFTB parameterization, the localized basis functions of valence orbitals for the confined pseudo-atom were calculated with all-electron DFT (in Hotbit). At the end of the first two steps, the Hamiltonian and overlap matrices for elementary integrals as a function of distance were

calculated once and for all for interaction of two atoms and stored in a parameter file (Slater–

Koster table).

Table 1. Electronic configurations and confinement potential parameters for Pt and Ru

Element	Valence Configuration	r_0(Bohr)	N	ε_d(Ha)	ε_p(Ha)	ε_s(Ha)	U_d(Ha)
Pt	$5d^9 6s^1 6p^0$	4.80	2	-0.235	-0.035	-0.218	0.367
Ru	$4d^7 5s^1 5p^0$	5.27	2	-0.199	-0.038	-0.166	0.356

In the third and final step, we fit the repulsive pairwise function, $V_{rep}(R_{IJ})$ that accounts for

ion-ion interaction and exchange-correlation effects. The parameters of this potential can be

optimized by fitting to a suitable training set. It is well known that DFTB approximations are

sufficiently crude so that training data from a single system result in poor transferability.[24] Thus

in order to achieve higher transferability, we model numerous clusters with different size and

geometries in DFT and use these data for training and testing purpose. As force (energy gradient)

minimization rather than energy minimization is the appropriate metric for structural

optimization, we define our objective function as $|\, F^{\text{DFT}}(R) - F^{\text{DFTB}}(R)|$, which is norm of the

force difference between DFT benchmarks and DFTB outputs.

Figure 1 displays the results of the training procedure as applied to Pt-Pt, Ru-Ru, and Pt-Ru

interactions. All training data are from DFT calulations with spin polarization; the DFTB

parameterization developed in this work does not include either spin polarization or spin-orbit

effects. To the extent that our goal is to simply employ DFTB for structural optimization rather

than detailed electronic structure calulations, this approach is similar in spirit to empirical

potential approaches. The training set employed here includes (strained) atomic dimers, which

we find to be very important in determining the shape of the repulsive potential curves over a

large range of interatomic distances. For larger clusters, we similarly employ both ground state

9

configurations as well as structures that are homogeneously expanded or contracted to sample a range of atomic environments. As seen from Fig. 1, the training procedure results in repulsive potentials that are in excellent agreement for both homo-elemental and alloy systems. In particular, we found that empirically tuning the d-orbital energies ε_d relative to their default DFT-calculated values (Table 1) has a significant effect on the quality of the data fits. Table S1
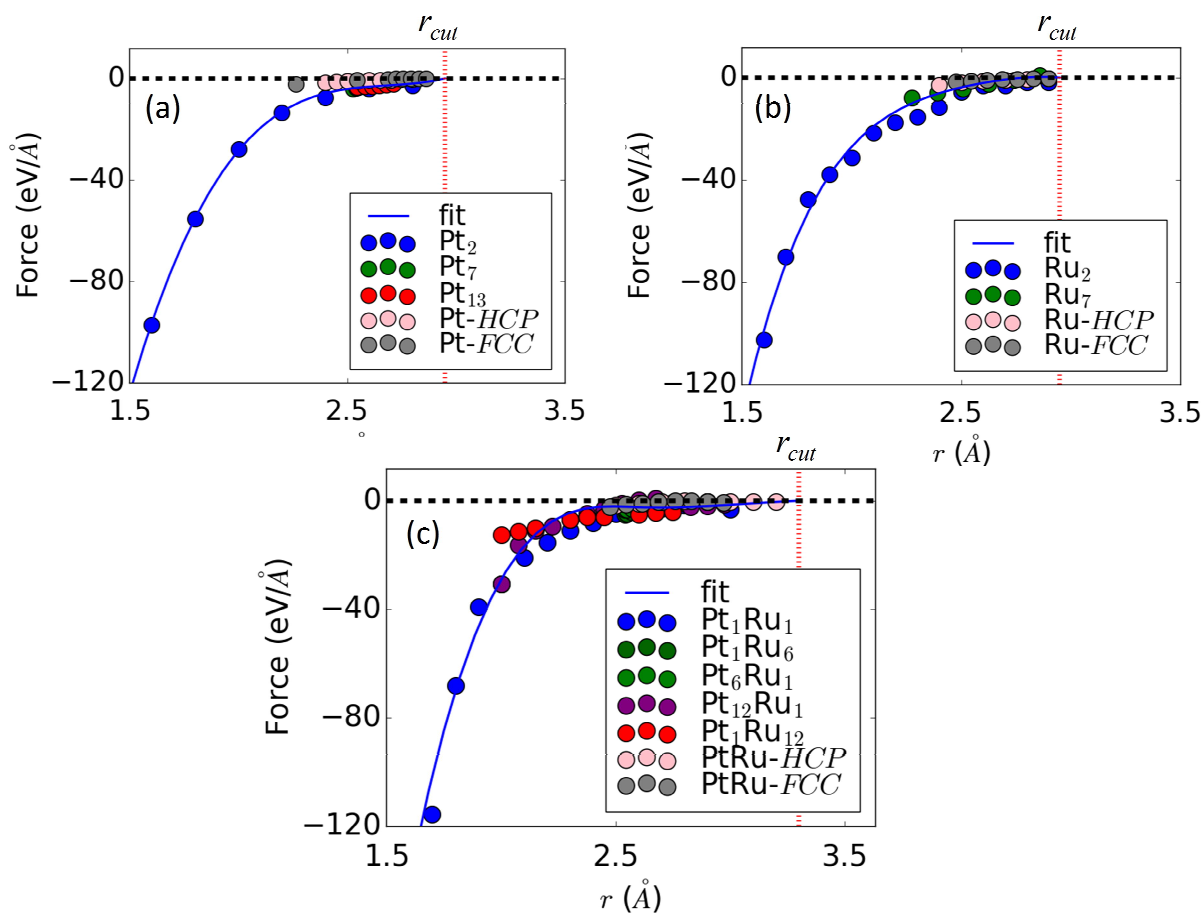

Figure 1: Fitting the derivatives of repulsive potential: (a): Pt-Pt interaction; (b): Ru-Ru interaction; (c): Pt-Ru interaction. Family of points are from various structures. The cutoff distance for the repulsive interaction is $r_{cut} = 3.3$ Å.

in the Supplementary information displays the results of this tuning exercise; Fig. 1 displays the results with optimal onset energies (-0.25 Ha for Pt and -0.24 Ha for Ru).

While we also attempted to include bulk data in the training set, this seemed to adversely

10

affect accuracy for clusters. Since our focus here is on modeling alloy clusters rather than bulk

systems, we chose not to include bulk data in the training sets. The transferability of the homo-

elemental parameterizations (Pt-Pt and Ru-Ru) from cluster data is nevertheless satisfactory for

bulk Pt and Ru systems as shown in Table S1; the transferability to bulk Pt-Ru alloys is, however,

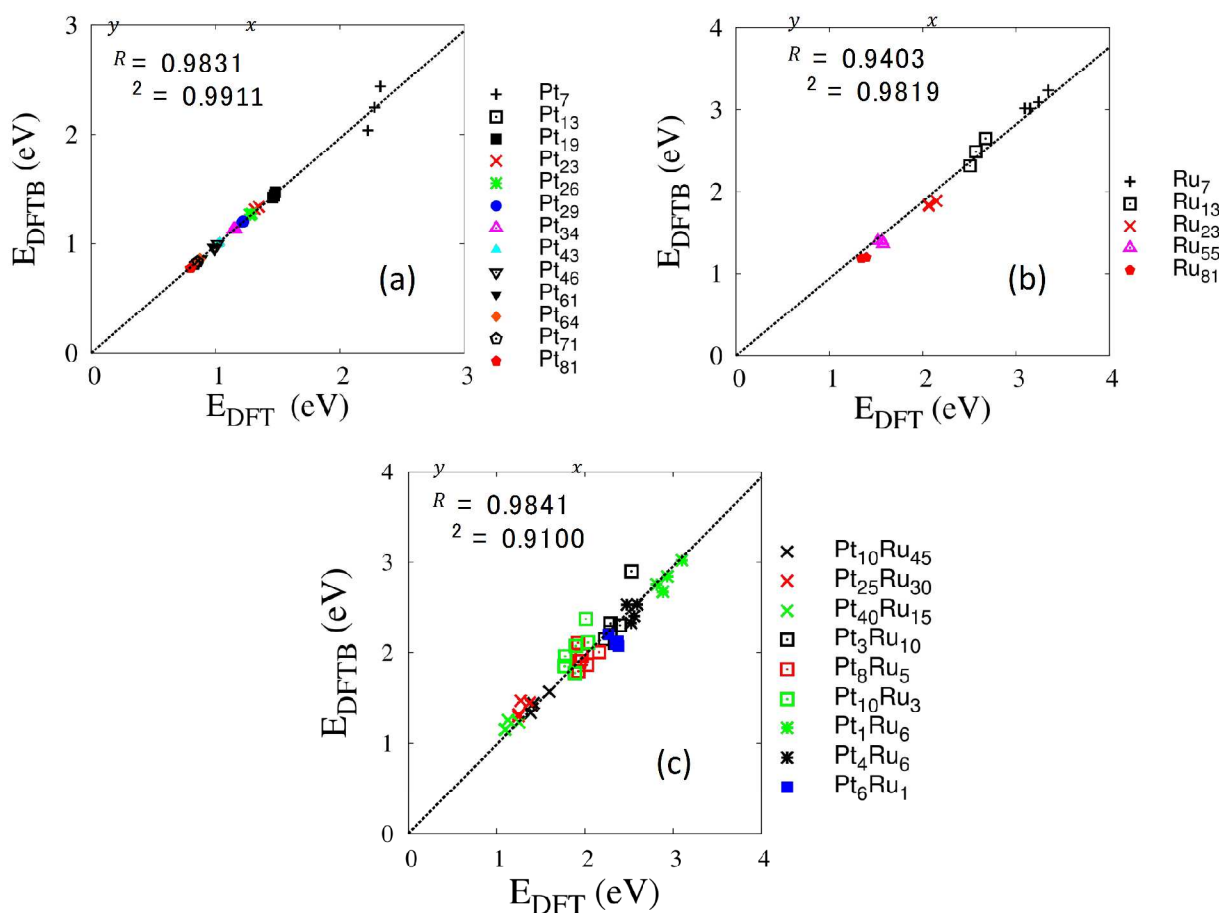poor and we caution against using this DFTB parameter set beyond clusters.

Figure 2: Comparison of DFT and DFTB formation energies of Pt, Ru and PtRu clusters. Dashed lines indicate the least-squares fit to the data. The slopes of the lines (ideally unity) and the R^2 values indicate an accurate DFTB representation of the target DFT data.

The quality of DFTB parameterization is tested by comparing cluster formation energies

calculated using both DFTB and DFT as shown in Fig. 2. The formation energy for a Pt_mRu_n

11

cluster (on a per atom basis) is defined as

$$E_f = [E(Pt_m Ru_n) - m\,E_{Pt} - n\,E_{Ru}]/(m+n), \tag{5}$$

where $E(Pt_m Ru_n)$ is the total energy of the cluster, and E_{Pt} and E_{Ru} are the energies per atom of bulk FCC Pt and HCP Ru, respectively. Test geometries for each size and composition are based on cluster morphologies from our previous study on Pt nanoclusters.[18] Ru and PtRu clusters are simply generated by replacing Pt atoms in these clusters and subjecting them to structural relaxation. In general, we see that for both homo-elemental as well as alloy clusters, the DFTB formation energies faithfully represent the target DFT data. Indeed, in addition to *R*-squared values being very close to one, indicating small statistical scatter, the slopes of the fits are also close to unity, indicating excellent one-to-one correspondence in the DFTB and DFT formation energies. Based on this successful parameterization, we pursue next a few examples of GA-based morphological optimization of PtRu alloy clusters.

3.2 DFTB-based Genetic Algorithm optimization of PtRu cluster morphologies

We now apply our new SCC-DFTB parameterization to the problem of ascertaining minimum-energy morphologies of PtRu clusters as a function of cluster size and composition. The goal here is not to undertake a detailed study of the structural and electronic properties of PtRu alloy clusters but simply to use the DFTB parameterization in conjunction with a GA to confirm experimentally observed features (see details below) of sub-nanometer PtRu clusters and validate the model. As examples, we consider PtRu clusters with 13, 32, 55, and 81 atoms with (approximate) Pt atomic fractions of   0%, 25%, 50%, 75% and 100% in each case. Figure 3 displays the various minimum-energy cluster morphologies for various cluster sizes and composition. As seen from Fig. 3, the clusters exhibit low-symmetry morphologies in all cases

12

with little or no resemblance to high-symmetry icosahedral or cuboctahedral geometries as is often assumed *ad hoc* in computational studies. In particular, the finding that low-energy Pt clusters typically adopt low-symmetry structures at small sizes is consistent with several prior studies.[18, 48, 49] In the case of PtRu alloy clusters, it is well known from several experimental studies[50, 51] that Pt atoms preferentially occupy surface sites whereas Ru atoms segregate towards
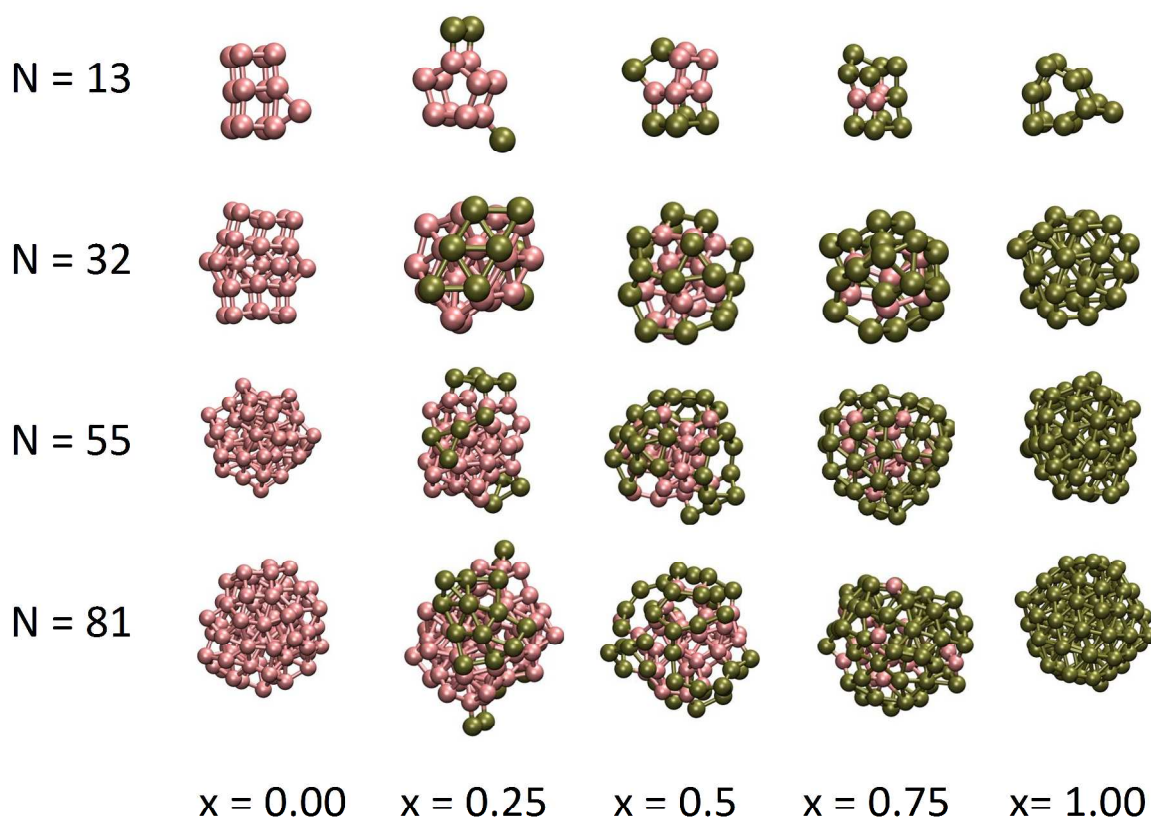

Figure 3: Morphologies of minimum-energy PtRu clusters of various sizes (N – number of atoms) and compositions (*x* – Pt fraction) as predicted by our DFTB-based GA implementation. Gold and pink spheres represent Pt and Ru atoms, respectively.

the core sites. This is also borne out by our simulations, as seen from Fig. 3, wherein we consistently find segregation of Pt atoms to the surface with (near) core–shell-like morphologies visible at intermediate Pt compositions. As noted by Wang et al.,[51] this segregation is a

13

mechanism for reducing the energetically unfavorable filling of antibonding states of Pt that occurs during alloying with Ru. One may also note that the cohesive energy of HCP Ru is much larger than that of FCC Pt (by 2.8 eV; Table S1), whereas the surface energies of typical low-index Miller surfaces of Ru are higher than that of Pt (Table S1); both of these facts would also point towards the tendency for phase segregation with Pt preferentially occupying surface sites.
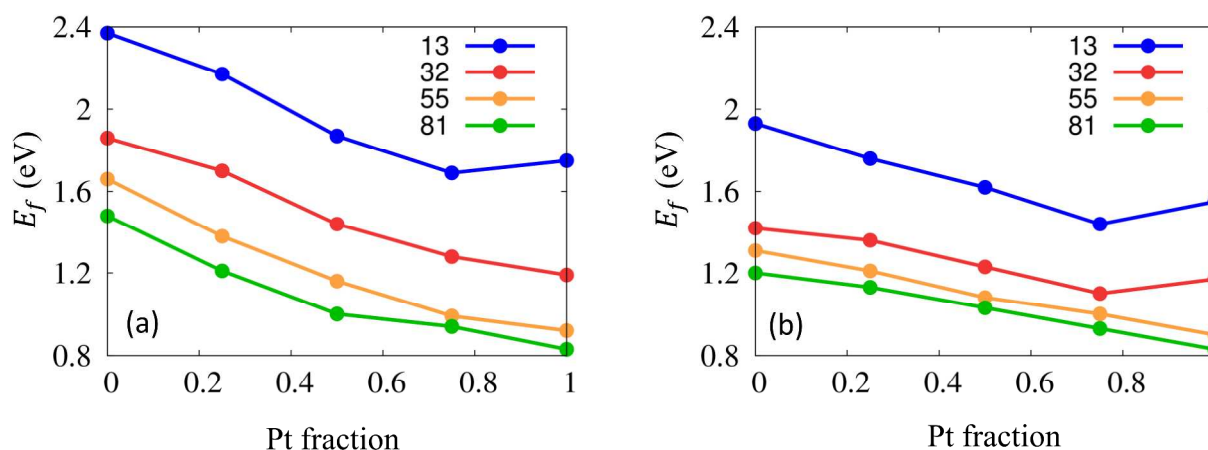

Figure 4. Formation energies of GA-optimized PtRu clusters (displayed in Fig. 3) as a function of Pt concentration, calculated with (a) DFT and (b) DFTB. Cluster sizes (number of atoms) are indicated in the legends.

As a quantitative comparison of the DFTB model against DFT, we display in Fig. 4 the formation energies of the GA-optimized clusters (Fig. 3). The DFTB results are obtained by the application of the GA; these GA-optimized clusters are simply imported into VASP and subjected to a conjugate-gradient structural relaxation (local energy minimization) after which formation energies are calculated using Eq. 5. In general, we see from Fig. 4 that at any given composition, smaller clusters have larger formation energies (less thermodynamically stable), which is to be expected due to the larger number of undercoordinated atoms in smaller clusters. For the 13-atom cluster, both DFTB and DFT predict a minimum formation energy at $x=0.75$.

14

For the 32-atom cluster, DFTB predicts a shallow minimum in formation energy at x=0.75, which is not captured in DFT. For larger clusters, the DFTB and DFT results agree in predicting a monotonic decrease in formation energy from pure Ru to pure Pt clusters. In general, DFTB tends to underestimate formation energies relative to DFT (on average, by about 0.41 eV/atom) although the overall trends are broadly captured. Nevertheless, to the extent that we propose to use DFTB as a "pre-processing" step to search the potential-energy hypersurface for low-energy candidates for subsequent higher-level DFT calculations, the agreement may be deemed satisfactory.

4. CONCLUSIONS

We have developed an SCC-DFTB parameterization that allows us to model chemical bonding in Pt-Ru alloy clusters. The parameter set was developed by using a training set of first-principles DFT data for homo-elemental (Pt and Ru) and alloy clusters. Our new parameterization is able to describe the thermodynamics (formation energies) of Pt, Ru, and PtRu nanoclusters in reasonable agreement with benchmark DFT calculations.

As an example application, we employed the validated DFTB parameter set within a Genetic Algorithm for structural optimization of PtRu clusters and showed that the procedure correctly captures surface segregation of Pt in PtRu nanoclusters. The low-energy structures predicted by the DFTB-based GA can serve as good starting points for future investigations of electronic properties and catalytic activity with higher-level DFT calculations. More broadly, the new DFTB parameter set for Pt-Ru interactions presented in this work opens up avenues for detailed investigation of structure–function relationships in this important class of catalytic materials.

15

SUPPORTING INFORMATION

The Supporting Information is available free of charge on the ACS Publications website at DOI: [to be inserted by publisher]

Structural and thermodynamic properties of bulk Pt and Ru phases; comparison of genetic algorithm and simulated annealing for structural optimization; Slater-Koster tables in DFTB+ format for Pt-Pt, Ru-Ru and Pt-Ru interactions

REFERENCES

(1). Yu, X. W.; Ye, S. Y. Recent advances in activity and durability enhancement of Pt/C catalytic cathode in PEMFC - Part II: Degradation mechanism and durability enhancement of carbon supported platinum catalyst. *J. Power Sources.* **2007**, *172*, 145-154.

(2). Zhang, S. S.; Yuan, X. Z.; Hin, J. N. C.; Wang, H. J.; Friedrich, K. A.; Schulze, M. A review of platinum-based catalyst layer degradation in proton exchange membrane fuel cells. *J. Power Sources.* **2009**, *194*, 588-600.

(3). Antolini, E.; Salgado, J. R. C.; Gonzalez, E. R. The stability of Pt-M (M = first row transition metal) alloy catalysts and its effect on the activity in low temperature fuel cells - A literature review and tests on a Pt-Co catalyst. *J. Power Sources.* **2006**, *160*, 957-968.

(4). Cheng, X.; Shi, Z.; Glass, N.; Zhang, L.; Zhang, J. J.; Song, D. T.; Liu, Z. S.; Wang, H. J.; Shen, J. A review of PEM hydrogen fuel cell contamination: Impacts, mechanisms, and mitigation. *J. Power Sources.* **2007**, *165*, 739-756.

(5). Wen, Z. H.; Liu, J.; Li, J. H. Core/shell Pt/C nanoparticles embedded in mesoporous carbon as a methanol-tolerant cathode catalyst in direct methanol fuel cells. *Adv. Mater.* **2008**, *20*, 743-747.

(6). Yoo, E.; Okata, T.; Akita, T.; Kohyama, M.; Nakamura, J.; Honma, I. Enhanced electrocatalytic activity of Pt subnanoclusters on graphene nanosheet surface. *Nano Lett.* **2009**, *9*, 2255-2259.

(7). Li, Y. J.; Gao, W.; Ci, L. J.; Wang, C. M.; Ajayan, P. M. Catalytic performance of Pt nanoparticles on reduced graphene oxide for methanol electro-oxidation. *Carbon.* **2010**, *48*, 1124-1130.

(8). Xu, C. X.; Wang, L.; Mu, X. L.; Ding, Y. Nanoporous PtRu alloys for electrocatalysis. *Langmuir.* **2010**, *26*, 7437-7443.

(9). Travitsky, N.; Ripenbein, T.; Golodnitsky, D.; Rosenberg, Y.; Burshtein, L.; Peled, E. Pt-, PtNi- and PtCo-supported catalysts for oxygen reduction in PEM fuel cells. *J. Power Sources.* **2006**, *161*, 782-789.

(10). Yu, Y. C.; Xin, H. L. L.; Hovden, R.; Wang, D. L.; Rus, E. D.; Mundy, J. A.; Muller, D. A.; Abruna, H. D. Three-dimensional tracking and visualization of hundreds of Pt-Co fuel cell nanocatalysts during electrochemical aging. *Nano Lett.* **2012**, *12*, 4417-4423.

17

(11).Ball, S.; Hodgkinson, A.; Hoogers, G.; Maniguet, S.; Thompsett, D.; Wong, B. The proton exchange membrane fuel cell performance of a carbon supported PtMo catalyst operating on reformate. *Electrochem. Solid-State Lett.* **2002**, *5*, A31-A34.

(12).Mukerjee, S.; Lee, S. J.; Ticianelli, E. A.; McBreen, J.; Grgur, B. N.; Markovic, N. M.; Ross, P. N.; Giallombardo, J. R.; De Castro, E. S. Investigation of enhanced CO tolerance in proton exchange membrane fuel cells by carbon supported PtMo alloy catalyst. *Electrochem. Solid-State Lett.* **1999**, *2*, 12-15.

(13).Krausa, M.; Vielstich, W. Study of the electrocatalytic influence of Pt/Ru and Ru on the oxidation of residues of small organic-molecules. *J. Electroanal. Chem.* **1994**, *379*, 307-314.

(14).Tong, Y. Y.; Kim, H. S.; Babu, P. K.; Waszczuk, P.; Wieckowski, A.; Oldfield, E. An NMR investigation of CO tolerance in a Pt/Ru fuel cell catalyst. *J. Am. Chem. Soc.* **2002**, *124*, 468-473.

(15).Gasteiger, H. A.; Markovic, N.; Ross, P. N.; Cairns, E. J. Methanol electrooxidation on well-characterized platinum-ruthenium bulk alloys. *J. Phys. Chem.* **1993**, *97*, 12020-12029.

(16).Johnston, R. L. Evolving better nanoparticles: Genetic algorithms for optimising cluster geometries. *Dalton Trans.* **2003**, 4193-4207.

(17).Rossi, G.; Ferrando, R.; Rapallo, A.; Fortunelli, A.; Curley, B. C.; Lloyd, L. D.; Johnston, R. L. Global optimization of bimetallic cluster structures. II. Size-matched Ag-Pd, Ag-Au, and Pd-Pt systems. *J. Chem. Phys.* **2005**, *122*, 194308.

(18).Shi, H. B.; Auerbach, S. M.; Ramasubramaniam, A. First-principles predictions of structure function relationships of graphene-supported platinum nanoclusters. *J. Phys. Chem. C.* **2016**, *120*, 11899-11909.

(19).Tekin, A.; Hartke, B. Global geometry optimization of small silicon clusters with empirical potentials and at the DFT level. *PCCP.* **2004**, *6*, 503-509.

18

(20). Wang, X. L.; Tian, D. X. Structures and structural evolution of Pt-n (n=15-24) clusters with combined density functional and genetic algorithm methods. *Comput. Mater. Sci.* **2009**, *46*, 239-244.

(21). Davis, J. B. A.; Horswell, S. L.; Johnston, R. L. Global optimization of 8-10 atom Palladium-Iridium nanoalloys at the DFT Level. *J. Phys. Chem. A.* **2014**, *118*, 208-214.

(22). Porezag, D.; Pederson, M. R.; Frauenheim, T.; Kohler, T. Structure, stability, and vibrational properties of polymerized C-60. *Phys. Rev. B.* **1995**, *52*, 14963-14970.

(23). Porezag, D.; Frauenheim, T.; Kohler, T.; Seifert, G.; Kaschner, R. Construction of tight-binding-like potentials on the basis of density-functional theory: application to carbon. *Phys. Rev. B.* **1995**, *51*, 12947-12957.

(24). Koskinen, P.; Makinen, V. Density-functional tight-binding for beginners. *Comput. Mater. Sci.* **2009**, *47*, 237-253.

(25). Koskinen, P.; Hakkinen, H.; Seifert, G.; Sanna, S.; Frauenheim, T.; Moseler, M. Density-functional based tight-binding study of small gold clusters. *New J. Phys.* **2006**, *8*.

(26). Makinen, V.; Koskinen, P.; Hakkinen, H. Modeling thiolate-protected gold clusters with density-functional tight-binding. *Eur. Phys. J. D.* **2013**, *67*.

(27). Elstner, M.; Frauenheim, T.; Kaxiras, E.; Seifert, G.; Suhai, S. A self-consistent charge density-functional based tight-binding scheme for large biomolecules. *Phys. Status Solidi B.* **2000**, *217*, 357-376.

(28). Elstner, M.; Porezag, D.; Jungnickel, G.; Elsner, J.; Haugk, M.; Frauenheim, T.; Suhai, S.; Seifert, G. Self-consistent-charge density-functional tight-binding method for simulations of complex materials properties. *Phys. Rev. B.* **1998**, *58*, 7260-7268.

(29). https://trac.cc.jyu.fi/projects/hotbit (accessed by February 07, 2017).

19

(30).Aradi, B.; Hourahine, B.; Frauenheim, T. DFTB+, a sparse matrix-based implementation of the DFTB method. *J. Phys. Chem. A.* **2007**, *111*, 5678-5684.

(31).Kresse, G.; Furthmuller, J. Efficiency of ab-initio total energy calculations for metals and semiconductors using a plane-wave basis set. *Comput. Mater. Sci.* **1996**, *6*, 15-50.

(32).Kresse, G.; Furthmuller, J. Efficient iterative schemes for ab initio total-energy calculations using a plane-wave basis set. *Phys. Rev. B.* **1996**, *54*, 11169-11186.

(33).Perdew, J. P.; Yue, W. Accurate and simple density functional for the electronic exchange energy-generalized gradient approximation. *Phys. Rev. B.* **1986**, *33*, 8800-8802.

(34).Perdew, J. P.; Burke, K.; Ernzerhof, M. Generalized gradient approximation made simple. *Phys. Rev. Lett.* **1996**, *77*, 3865-3868.

(35).Perdew, J. P.; Burke, K.; Wang, Y. Generalized gradient approximation for the exchange-correlation hole of a many-electron system. *Phys. Rev. B.* **1996**, *54*, 16533-16539.

(36).Methfessel, M.; Paxton, A. T. High-precision sampling for brillouin-zone integration in metals. *Phys. Rev. B.* **1989**, *40*, 3616-3621.

(37).Priest, C.; Tang, Q.; Jiang, D. E. Structural evolution of Tc-n (n=4-20) clusters from first-principles global minimization. *J. Phys. Chem. A.* **2015**, *119*, 8892-8897.

(38).Ouyang, R. H.; Xie, Y.; Jiang, D. E. Global minimization of gold clusters by combining neural network potentials and the basin-hopping method. *Nanoscale.* **2015**, *7*, 14817-14821.

(39).Hamad, S.; Catlow, C. R. A.; Woodley, S. M.; Lago, S.; Mejias, J. A. Structure and stability of small TiO2 nanoparticles. *J. Phys. Chem. B.* **2005**, *109*, 15741-15748.

(40).Gould, A. L.; Heard, C. J.; Logsdail, A. J.; Catlow, C. R. A. Segregation effects on the properties of (AuAg)147. *PCCP.* **2014**, *16*, 21049-21061.

20

(41).Arslan, H. Structures and energetic of Palladium-Cobalt binary clusters. *Int. J. Mod. Phys. C.* **2008**, *19*, 1243-1255.

(42).Lv, J.; Wang, Y. C.; Zhu, L.; Ma, Y. M. Particle-swarm structure prediction on clusters. *J. Chem. Phys.* **2012**, *137*, 084104.

(43).Gies, D.; Rahmat-Samii, Y. Particle swarm optimization for reconfigurable phase-differentiated array design. *Microw. Opt. Technol. Lett.* **2003**, *38*, 168-175.

(44).Lloyd, L. D.; Johnston, R. L.; Roberts, C.; Mortimer-Jones, T. V. Geometry optimisation of aluminium clusters using a genetic algorithm. *Chemphyschem.* **2002**, *3*, 408-415.

(45).Zhao, J. J.; Xie, R. H. Genetic algorithms for the geometry optimization of atomic and molecular clusters. *J. Comput. Theor. Nanosci.* **2004**, *1*, 117-131.

(46).Perdew, J. P.; Wang, Y. Accurate and simple analytic representation of the electron-gas correlation-energy. *Phys. Rev. B.* **1992**, *45*, 13244-13249.

(47).Frauenheim, T.; Porezag, D.; Elstner, M.; Jungnickel, G.; Elsner, J.; Haugk, M.; Sieck, A. An ab initio two-center tight-binding approach to simulations of complex materials properties. *Mater Res Soc Symp P.* **1998**, *491*, 91-104.

(48).Fampiou, I.; Ramasubramaniam, A. Binding of Pt nanoclusters to point defects in graphene: adsorption, morphology, and electronic structure. *J. Phys. Chem. C.* **2012**, *116*, 6543-6555.

(49).Kumar, V.; Kawazoe, Y. Evolution of atomic and electronic structure of Pt clusters: Planar, layered, pyramidal, cage, cubic, and octahedral growth. *Phys. Rev. B.* **2008**, *77*, 205418.

(50).Gasteiger, H. A.; Ross, P. N.; Cairns, E. J. LEIS and AES on sputtered and annealed polycrystalline Pt-Ru bulk alloys. *Surf. Sci.* **1993**, *293*, 67-80.

(51).Wang, L. L.; Khare, S. V.; Chirita, V.; Johnson, D. D.; Rockett, A. A.; Frenkel, A. I.; Mack, N. H.; Nuzzo, R. G. Origin of bulklike structure and bond length disorder of Pt37 and Pt6Ru31

21

clusters on carbon: Comparison of theory and experiment. *J. Am. Chem. Soc.* **2006**, *128*, 131-

142.
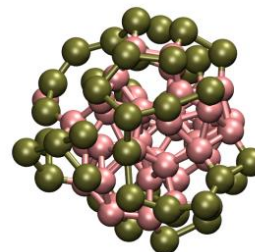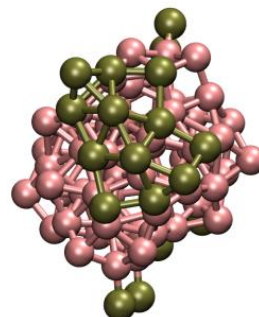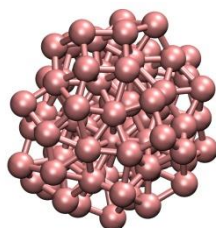
1
2
3
4
5
6
7
8
9
10
11
12
13
14
15
16
17
18
19
20
21
22
23
24
25
26
27
28
29
30
31
32
33
34
35
36
37
38
39
40
41
42
43
44
45
46
47
48
49
50
51
52
53
54
55
56
57
58
59
60

Table of Contents Figure

N = 13

N = 32

N = 55

N = 81

x = 0.00   x = 0.25   x = 0.5   x = 0.75   x= 1.00